Facile Fabrication of Flexible and Porous Single-Walled Carbon Nanotubes/Polyaniline Composite Films via a Novel Solution Approach for Supercapacitor Applications

Fuwei Liu,* Hongbing Ge, Feng Gao, Jingxian Li, Minrui Li, Yuan Liu, Jianshu Zhang, Meilin Li, Yaxin Wang, Minshen Zhu,* and Yang Huang*

Due to their potential of fast and reversible redox reaction, carbon nanotubes/polyaniline (CNTs/PANI) composites are receiving increasing attention as promising electrode for supercapacitors (SCs). This study explores a facile "direct-immersion" approach for fabricating single-walled CNTs (SWCNTs)/PANI flexible composite films for SCs. PANI is dissolved in concentrated sulfuric acid (H_2SO_4) to form a conducting ink, into which the SWCNTs film is soaked. The concentrated H_2SO_4 promotes effective contact between PANI and CNTs, forming stable SWCNT/PANI interface through strong π–π interactions. By controlling reaction conditions, the structural integrity and supercapacitive performance of SWCNT/PANI are improved. Prolonging the immersion time to 24 h results in a flake-like structure of PANI, with CNTs linking among the flakes. This configuration facilitates ion transport and realizes fast redox reactions. Consequently, a high specific capacitance of 329 F g^{-1} (at 1 A g^{-1}) is achieved, demonstrating good rate capability and cycling stability. Moreover, the as-assembled SC devices achieve a high energy density of 14 Wh kg^{-1} at a power density of 400 W kg^{-1}. These devices exhibit remarkable electrochemical durability, without occurring obvious capacitance deterioration after 5000 charge/discharge. This work paves the way for the design and fabrication of high-performance PANI-based SCs.

1. Introduction

In response to the growing demand for powerful portable electronics, flexible energy storage systems with compact configurations have emerged as principal power sources.[1] In particular, supercapacitors (SCs) stand out for their high power density, long cycling life, and fast charging/discharging capabilities.[2] Nevertheless, their energy density remains insufficient, hindering their further development in portable device applications. To address this dilemma, various materials have been extensively investigated as electrode candidates for SCs, such as carbon-based materials,[1c,3] metal oxides/hydroxides,[4] and conducting polymers.[5] Among these, polyaniline (PANI), a conductive polymer, has garnered significant research interest because of its high faradaic pseudocapacitance, environmental friendliness, affordability, and ease of processing. However, conventional PANI requires a current collector to significantly enhance its electrical conductivity, leading to a bulky appearance and increased weight. In addition, PANI exhibits poor rate capability and low cycling stability due to structural collapse during charging and discharging, reducing its potential for flexible SCs.

To overcome these limitations, a promising approach is to develop composite materials by incorporating PANI with conductive and flexible substrates to form integrated electrodes, such as active carbon, carbon nanotubes (CNTs), reduced graphene oxide, and MXene. Specifically, CNTs, including single-walled CNTs (SWCNTs) and multiwalled CNTs (MWCNTs), have been widely studied as potential additives to PANI for fabricating composite electrodes.[6] The incorporation of CNTs into PANI creates a composite that combines the high electrical conductivity of CNTs with the pseudocapacitive properties of PANI, facilitating faster charge transfer by reducing the internal resistance of the electrode. This leads to improved rate capability and cycling stability. For example, a robust and flexible PANI/MWCNT/(PVC) polyvinyl chloride composite film has been developed as a high-performance SC electrode. In this design, PANI is deposited through in situ chemical oxidative polymerization of aniline on the MWCNT/PVC composite film, where PVC acts as a supporting substrate.[7] The resulting composite film displays excellent electrochemical performance along with flexibility. Besides, a ternary composite of reduced graphene oxide/unzipped carbon nanotubes/polyaniline (RGO/UCNTs/PANI) with special 3D structures was constructed through an in situ polymerization.[8]

F. Liu, H. Ge, F. Gao, J. Li, M. Li, Y. Liu, J. Zhang
Key Laboratory of Microelectronics and Energy of Henan Province
College of Physics and Electronic Engineering
Xinyang Normal University
Xinyang 464000, Henan, P. R. China
E-mail: liufw@xynu.edu.cn

M. Li, Y. Wang, Y. Huang
Advanced Materials Thrust
The Hong Kong University of Science and Technology (Guangzhou)
Nansha, Guangzhou 511400, Guangdong, P. R. China
E-mail: yanghuang@hkust-gz.edu.cn

M. Zhu
Research Center for Materials
Architectures and Integration of Nanomembranes (MAIN)
Chemnitz University of Technology
09126 Chemnitz, Germany
E-mail: minshen.zhu@main.tu-chemnitz.de

The composite electrode possessed a specific capacitance of 359.3 F g^{-1} at a current density of 1 A g^{-1}, with a good cycling stability, retaining 80.5% of the original capacitance after 2000 cycles. Moreover, a "skeleton/skin" strategy was developed to fabricate freestanding, thin, and flexible SWCNT/PANI hybrid films, in which, SWCNT film with a continuous reticulate structure was used as templates.[9] The high electrical conductivity and flexibility, coupled with their continuous porous architecture, endow them with high SC performance, exhibiting high energy density (131 Wh kg^{-1}) and power density (62.5 kW kg^{-1}). Another similar wearable SC was achieved based on a PANI/N-CNT@CNT fiber with hierarchical structure, where PANI was electrochemically deposited in situ onto N-CNTs to achieve high specific capacitance.[5d] The porous N-CNT structure significantly facilitates electron and ion transfer, while the synergistic effects of the components contribute to the fiber's high specific capacitance (323.8 F g^{-1} at a current density of 1 A g^{-1}), excellent rate capability, and cycling stability. Despite these advantages, most of these approaches rely on in situ chemical and electrochemical polymerization, which poses challenges for large-scale applications due to the requirement of complex steps and delicate device.

To address this issue, an ingenious "direct-immersion" approach was employed to prepare flexible SWCNTs/PANI composite films. The process involves dissolving PANI in concentrated sulfuric acid (H$_2$SO$_4$) to prepare a conducting ink, into which the SWCNTs film is directly soaked. The concentrated H$_2$SO$_4$ facilitates effective contact between PANI molecules and CNTs due to the strong molecular interactions, further resulting in strong surface adhesion. Upon the introduction of water molecules, PANI gradually precipitates from H$_2$SO$_4$ and forms novel nanostructures on the nanotube walls, resulting in a distinct SWCNTs/PANI composite film. Notably, a simple adjustment of the reaction parameters can tailor the microstructure of electrode materials and modify their electrochemical properties. For example, flake-like PANI nanostructures with nanoscale pores appear after immersion for 24 h at 25 °C. At the same time, CNTs retain their original conductive skeleton. In this structure, PANI adopts a flake-like morphology, whereas the CNTs form connections between the flakes, facilitating ion transport and enabling fast redox reactions. As a result, a specific capacitance as high as 329 F g^{-1} is achieved for SWCNTs/PANI, substantially exceeding the performance of PANI alone (43.1 F g^{-1}) and that of SWCNTs (56.7 F g^{-1}) in a 1 M H$_2$SO$_4$ electrolyte. Additionally, a SC assembled using the SWCNTs/PANI electrode demonstrates a high energy density of 14 Wh kg^{-1} at a power density of 400 W kg^{-1}, along with excellent electrochemical durability, thereby outperforming many comparable SC devices. Compared with the conventional in situ polymerization techniques,[10] our novel solution approach demonstrates pronounced advantages in large-scale applications.

2. Results and Discussion

In this work, PANI was first prepared according to the conventional oxidative polymerization method, as shown in Figure S1, Supporting Information, which involves the oxidation of aniline monomers in the presence of an oxidizing agent, leading to the formation of PANI chains. Following the synthesis, PANI was directly dissolved in concentrated sulfuric acid (H$_2$SO$_4$). To ensure a homogeneous solution, the mixture was subjected to ultrasonic treatment for 2 h, which promotes the dispersion of PANI particles (as shown in Figure S2, Supporting Information) and helps to break down any agglomerates that may have formed. The SWCNTs/PANI composite electrode material is fabricated through a straightforward method involving the direct soaking of the CNTs film in the pre-prepared PANI-H$_2$SO$_4$ solution (**Figure 1**). Subsequently, water is sprayed onto the film, facilitating the gradual formation of the composite structure as PANI dissolves and interacts with CNTs. More details of the fabrication process have been discussed in the Experimental Section. The resulting composite exhibits a unique morphology (**Figure 2**) that promotes effective charge transfer and ion diffusion, which are critical for high-performance electrode materials in energy storage devices.
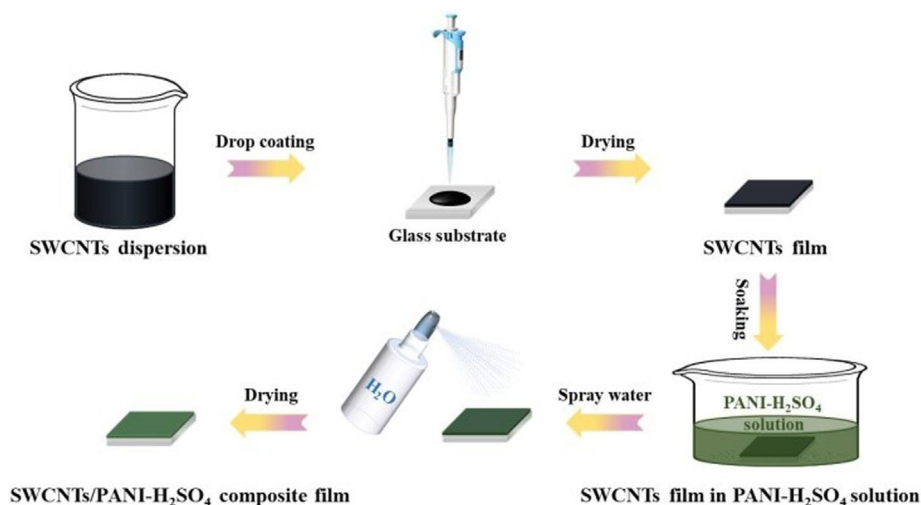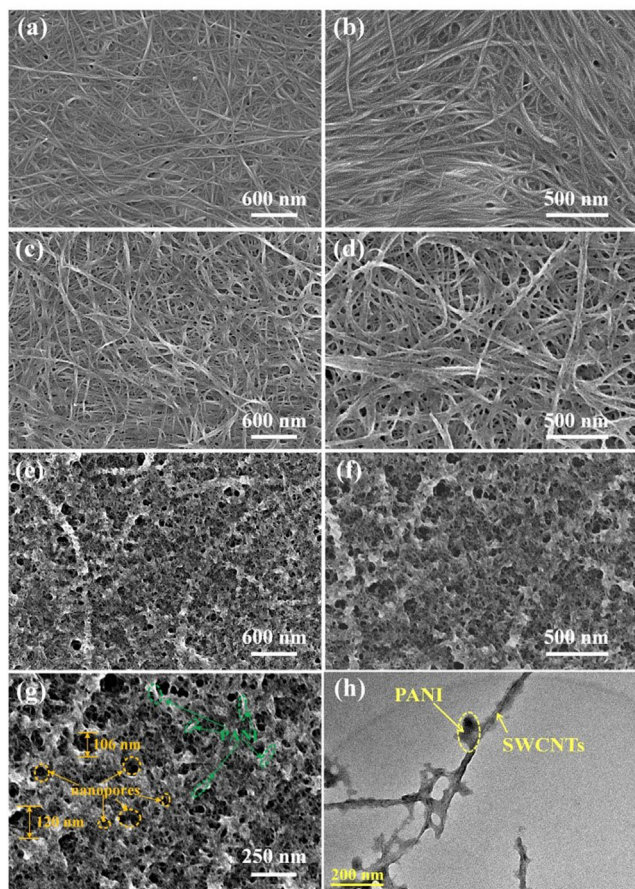

Figure 1. A scheme for the preparation of SWCNTs/PANI flexible composite film.
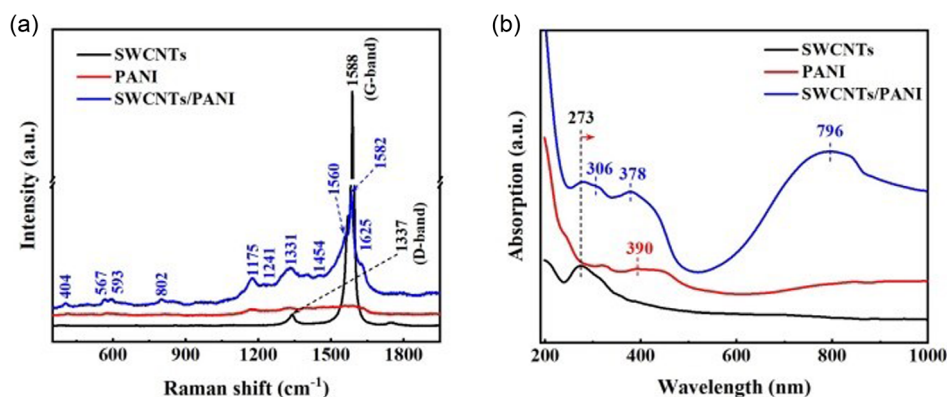
Figure 2. SEM and TEM micrographs of samples: a,b) SEM images of SWCNTs film; c,d) SEM images of the SWCNTs/PANI composite film fabricated through 4 h immersion in PANI-H$_2$SO$_4$ solution, and e–g) the one immersion for 24 h; h)TEM image of the sample immersion for 24 h.

The morphologies of the electrodes were observed using scanning electron microscopy (SEM). The SEM images show that the CNTs are uniformly distributed throughout the film (Figure 2a,b). After soaking in PANI-H$_2$SO$_4$ solution at 25 °C for 4 h, the surface of the SWCNTs becomes rough, with some PANI nanostructures adhere to their surface (Figure 2c,d). Extending the immersion time to 24 h results in a more porous, flake-like PANI, increasing the electrochemically active sites

(Figure 2e–g). Transmission electron microscopy (TEM) was also utilized to analyze the morphological features. As depicted in Figure 2h and S3, Supporting Information, some flake-like PANI nanostructures uniformly are distributed around the CNTs, with lateral dimensions ranging from around 20 to 109 nm. The resultant porous architecture with tunable pore sizes (20–120 nm, Figure 2g) will facilitate electrolyte penetration, while increasing electrochemically active sites. Moreover, effective connections are formed between SWCNTs and flake-like PANI, providing a rapid pathway for electrolyte ions transport and thus enhancing the electrochemical performance.[11] With increasing soaking time, a greater number of PANI nanostructures are observed on the sample surface. After 48 h of soaking, the CNTs surface is nearly fully covered with PANI, leading to a significant reduction in nanopores (Figure S4, Supporting Information). This coating could inhibit effective interface between PANI and electrolyte, thereby hindering fast redox reactions. Further discussion of this aspect will be provided later in this work.

Raman spectroscopy is a widely utilized technique for characterizing the structural and electronic properties of carbon materials and their composites.[12] As shown in **Figure 3**a, the spectra reveal structural changes in the SWCNTs/PANI freestanding film. The SWCNTs film exhibits two main characteristic peaks centered at 1337 and 1588 cm^{-1}, corresponding to the D band (associated with disordered defect structures) and the G band (sp2-bonded carbon atoms), respectively.[13] Following the growth of PANI, the Raman spectrum of SWCNTs/PANI shows significant differences compared to the precursor, with several new peaks indicating the existence of PANI (Table S1, Supporting Information), which is consistent with energy dispersive spectrometer results (Figure S5, Supporting Information). Specifically, the peaks at 404 and 567 cm^{-1} are assigned to the out-of-plane ring band of PANI,[14] while the peaks at 593 and 802 cm^{-1} are characteristic of benzenoid ring deformation and out-of-plane vibrations of aromatic rings, respectively.[14a,14b] Additionally, other peaks of PANI are observed in the composite film. The peak at 1175 cm^{-1} is associated with the C—H vibration, whereas the peak at 1241 cm^{-1} corresponds to the C—N stretching vibration. The peak at 1331 cm^{-1} is related to the C—N$^+$ vibration of the quinoid ring, and the peak at 1454 cm^{-1} is attributed to the C=N vibration of the diimine units. Furthermore, peaks at 1560

Figure 3. a) Raman and b) UV–Vis–NIR spectra for SWCNTs, PANI and SWCNTs/PANI films.

Batteries & Supercaps

Research Article
doi.org/10.1002/batt.202500063

**Chemistry
Europe**
European Chemical
Societies Publishing

and 1582 cm^{-1} represent C=C stretching of the quinoid ring and C—C stretching of the semiquinoid ring, respectively. Finally, the peak at 1625 cm^{-1} corresponds to the vibration of delocalized polarons in the extended polymeric conformation.[14b,14c,15] The presence of the emeraldine salt form of PANI, which provides sufficient charge carriers in SWCNTs/PANI, promotes fast redox reactions and enhances capacitance performance.[14c] Notably, certain peaks exhibit slight shifts compared to those of pure PANI. The C—N$^+$ vibration of the quinoid ring of pure PANI at 1333 cm^{-1}, shifts to a lower wavenumber (1331 cm^{-1}), whereas the C—H stretching vibration peak at 1167 cm^{-1} shifts to a higher wavenumber (1175 cm^{-1}), with significantly increased intensity. Moreover, the C=C stretching of the quinoid ring (1560 cm^{-1}) and the C—C stretching of the semiquinoid ring (1582 cm^{-1}) exhibit increased peak intensity, indicating the formation of additional quinoid ring-related bonds (Figure S6, Supporting Information). This is attributed to strong π–π conjugation interactions between PANI molecular chains and SWCNTs.[16] The presence of more "expanded coils" of PANI in the SWCNTs/PANI composite film enhances carrier mobility, facilitating the formation of a continuous conductive network. This feature improves capacitance, as a greater number of functional groups are involved in redox reactions during charging and discharging.[16,17]
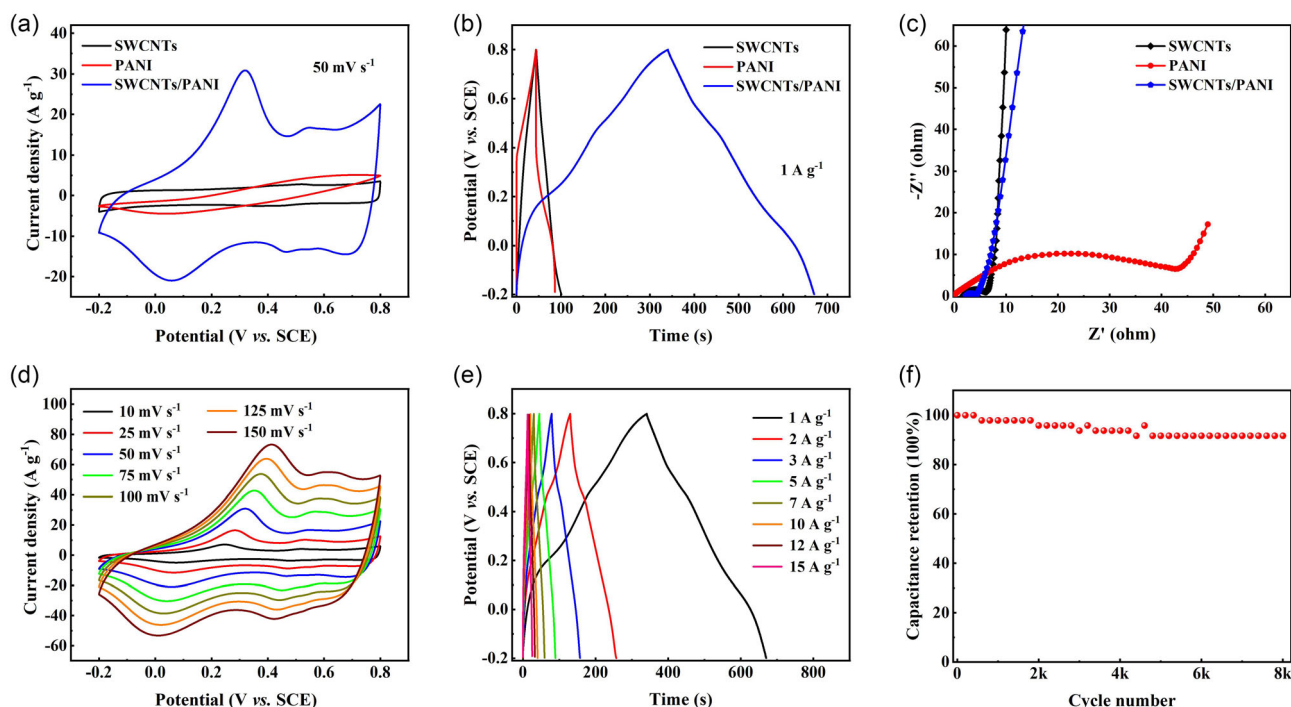
Ultraviolet–visible–near-infrared (UV–Vis–NIR) absorption spectra were used to analyze the compositional changes in the SWCNTs/PANI nanocomposites as well. As displayed in Figure 3b, the characteristic peak of SWCNTs centered at 273 nm corresponds to the π plasmon and is associated with the collective excitations of π electrons.[18] Upon the growth of PANI, the peak at 273 nm shifts to 280 nm, suggesting a strong interaction between SWCNTs and PANI. Additionally, three new absorption peaks appear at 306, 378, and 796 nm, which can be assigned to the $\pi \rightarrow \pi^*$, polaron $\rightarrow \pi^*$, and $\pi \rightarrow$ polaron transitions, respectively.[19] Apparently, the PANI as grown on SWCNT are highly doped with H$_2$SO$_4$ that facilitates the transport of charge carriers. Compared to pristine PANI (Figures 3b), the relative peak positions show slight shifts. Particularly, the characteristic polaron $\rightarrow \pi^*$ peak is blue-shifted from 390 to 378 nm, suggesting strong interactions between the two components. The interactions lead to a more uniform distribution of PANI on the SWCNTs, which is beneficial for achieving a high surface area with effective charge transfer pathways.

Next, X-ray photoelectron spectroscopy (XPS) measurements were conducted to investigate the variation in bonding states and their potential effects on capacitive performance. As shown in **Figure 4**a, the presence of C, N, O, and S in the full-scan spectra of the PANI and SWCNTs/PANI film samples confirms the successful formation of PANI on the CNTs surface. For pure PANI, the N 1s spectrum can be resolved into four distinct peaks corresponding to quinoid imines (399.5 eV), benzenoid imines (400.1 eV), positively charged imines (401.3 eV), and protonated amines (402.1 eV), as depicted in Figure 4b.[20] Notably, the N 1s peak (Figure S7, Supporting Information) of the SWCNTs/PANI composite slightly shifts toward lower binding energy compared to that of pure PANI, resulting from an increase in the intensity of the quinoid imine (—N=) peak located at 399.5 eV (Figure 4c). The presence of abundant quinoline imine (—N=) contributes to the high conductivity of PANI chains through electron delocalization. Moreover, a significant increase in peak area is noted for positively charged imines (401.3 eV) and protonated amines (402.1 eV). An increased N$^+$/N ratio indicates a higher doping level in PANI, signifying the presence of more unsaturated bonds in the SWCNTs/PANI films than in the pristine PANI films. This enhancement results in a greater average charge transfer number and improved electrochemical performance.[20,21] In accordance with the Raman results, these observations suggest the formation of strong π–π interactions between PANI and SWCNTs. In addition, the peak at 168.1 eV in the full-scan spectrum indicates the incorporation of SO$_4^{2-}$ in PANI (Figure 4a and S8, Supporting Information, originates from concentrated sulfuric acid, a prominent marker of successful sulfonation. More detailed discussion can be found in the Supporting Information), agrees well with Fourier transform infrared spectroscopy (FTIR) results (Figure S9, Supporting Information), leading to numerous unsaturated bonds and substantial reactive sites for redox reactions.

The as-prepared SWCNTs/PANI films exhibit flexibility and high conductivity, enabling their use as binder-free electrodes. **Figure 5**a presents the cyclic voltammetry (CV) curves of SWCNTs, SWCNTs/PANI, and PANI at a scan rate of 50 mV s^{-1} and a potential window from −0.2 to 0.8 V (vs saturated calomel electrode). The CV curve of the SWCNTs film electrode displays a quasi-rectangular shape, primarily attributed to electrochemical double-layer charging. The growth of PANI is characterized by
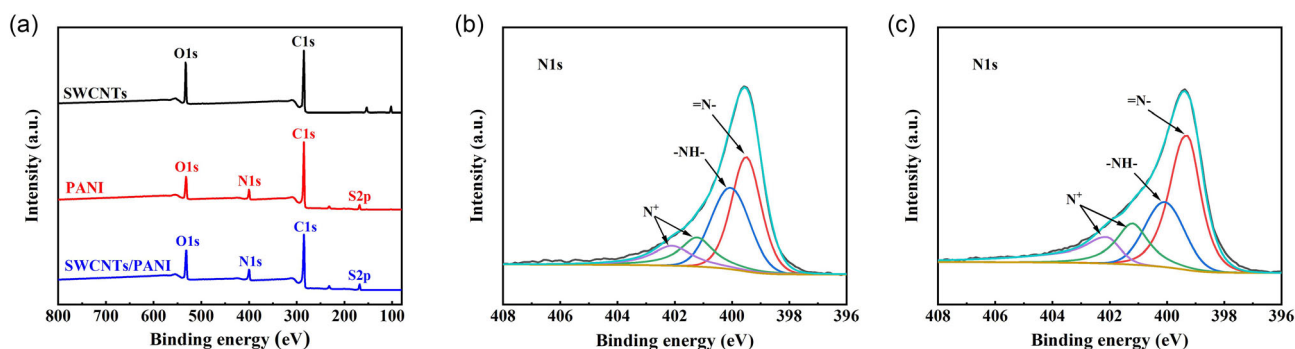
Figure 4. XPS spectra of SWCNTs, PANI, and SWCNTs/PANI: a) full-scale spectra, b) N1s spectra of pure PANI, and c) N1s of SWCNTs/PANI composite.

Batteries & Supercaps

Research Article
doi.org/10.1002/batt.202500063

Chemistry Europe
European Chemical
Societies Publishing

Figure 5. Electrochemical properties of SWCNTs, PANI, and SWCNTs/PANI electrodes: a) CV curves of samples at a scan rate of 50 mV s^{-1}; b) GCD curves of samples at a current density of 1 A g^{-1}; c) Nyquist plots of SWCNTs, PANI, and SWCNTs/PANI electrodes; d) CV curves of SWCNTs/PANI at different scan rates; e) GCD curves of SWCNTs/PANI at different current densities; f) cycle stabilities of SWCNTs/PANI during the long-term charging/discharging process.

the emergence of three redox peak couples in the CV curve, which can be ascribed to the redox transitions between leucoemeraldine and protonated emeraldine, p-benzoquinone and hydroquinone, and the Faradaic transformation between emeraldine and pernigraniline (Figure 5a). In contrast, pristine PANI electrodes show only subtle redox couples owing to their relatively poor electrical conductivity, hindering fast reversible redox reactions. The composite films, formed by PANI adhering to the surface of SWCNTs, create continuous conductive networks that facilitate ion transport and accelerate redox reactions, thus enhancing capacitive performance. Unsurprisingly, the CV curves of the SWCNTs/PANI films exhibit a much larger integrated area than those of the single-component samples, suggesting improved electrochemical properties. Additionally, the galvanostatic charge/discharge (GCD) curves demonstrate the benefits of the unique structure of the composite film. The curve of the SWCNTs/PANI composite film presents multiple stages of charge–discharge durations instead of a linear electric double-layer capacitance, revealing pseudocapacitance behavior attributed to the PANI nanostructures (Figure 5b). Moreover, compared to SWCNTs and conventional PANI, the SWCNTs/PANI composite displays a longer discharge period at the same current density (Figure 5b). Notably, the specific capacitance of the SWCNTs film is 56.7 F g^{-1}, which can be improved to 329 F g^{-1} after soaking in a PANI-H$_2$SO$_4$ solution for 24 h at 25 °C. This enhancement represents an increase of approximately eight times compared to traditional PANI powder, which has a capacitance of 43.1 F g^{-1}. Its remarkable capacitive performance is comparable to or even superior to that of other carbon-PANI electrodes (**Table 1**). For the sake of comparison, SWCNTs/PANI composites

were also prepared by in situ polymerization method in 1 M HCl. As depicted in Figure S10, Supporting Information, the specific capacitance of the reference sample is only 274.8 F g^{-1}. More detailed discussions have been given in the Supporting Information.

The growth conditions of PANI play a critical role in controlling the capacitance properties of the composite, with factors such as immersion time markedly influencing capacitance. Figure S11a, Supporting Information depicts the CV curves of the composite films at various PANI growth times at 25 °C. The shapes and enclosed areas of the CV curves vary significantly. With prolonged soaking time, the area of the CV curve gradually increases, reaching a maximum at 24 h. However, with a further increase in soaking time, the enclosed area of the curve decreases. The soaking time influences the surface morphology and conductivity of SWCNT/PANI (Figure S4, Supporting Information), leading to decreased electrochemical activity and reduced capacitance, as evidenced by the CV and GCD curves (Figure S11, Supporting Information). Meanwhile, the influence of immersion temperature was also investigated, and the results are shown in Figure S12, S13, Supporting Information. A detailed discussion is available in the Supporting Information.

Besides, electrochemical impedance spectroscopy (EIS) measurements were conducted, with the results presented in Figure 5c. The Nyquist curves for all samples exhibit a semicircle alongside an inclined straight line. The interception with the real axis at higher frequencies is indicative of the series resistance (Rs), which comprises the electrolyte resistance, the inherent resistance of the electrode material, and the contact resistance at the interface between the active material and the collector.

Batteries & Supercaps

Research Article
doi.org/10.1002/batt.202500063

Chemistry Europe
European Chemical
Societies Publishing

Table 1. Comparison of the electrochemical performances for various PANI-based nanocomposites as SC electrodes.

| Electrode materials	Electrolyte	Specific capacitance [F g^{-1}]	Capacitance retention [%]	Reference
Wood-derived porous carbon/PANI	1 M H_2SO_4	347 F g^{-1} at 2 A g^{-1}	67 (2500)	[26]
Bamboo carbon/PANI	1 M H_2SO_4	277 F g^{-1} at 0.5 A g^{-1}	92 (1000)	[27]
N-self-doped carbon framework/PANI	1 M H_2SO_4	373 F g^{-1} at 1 A g^{-1}	80 (5000)	[28]
PANI-CNT	1 M H_2SO_4	385 F g^{-1} at 0.5 A g^{-1}	81.4 (1000)	[29]
PANI/N-CNT@CNT	1 M H_2SO_4	323.8 F g^{-1} at 1 A g^{-1}	92.1 (10 000)	[5d]
MOF/PANI	1 M H_2SO_4	395.4 F g^{-1} at 0.2 A g^{-1}	–	[30]
PANI nanosphere/GO film	0.5 M H_2SO_4	448 F g^{-1} at 1 A g^{-1}	81 (5000)	[31]
RGO/UCNTs/PANI	1 M H_2SO_4	359.3 F g^{-1} at 1 A g^{-1}	80.5 (2000)	[8]
PANI/CNTs	1 M H_2SO_4	305.3 F g^{-1} at 1 mA cm^{-2}	54.1 (1000)	[6]
CMC-PANI/CNT	1 M H_2SO_4	348.8 F g^{-1} at 0.5 A g^{-1}	87.7 (5000)	[6]
PANI-doped graphene	2 M H_2SO_4	480 F g^{-1} at 0.1 A g^{-1}	70 (1000)	[32]
SWCNTs/PANI free-standing film	1 M H_2SO_4	329 F g^{-1} at 1 A g^{-1}	91.7 (8000)	This work

The radius of the semicircle reflects the charge transfer impedance (R_{ct}). For the pristine SWCNTs film, charge transfer impedance is measured at 4.5 Ω, which decreases to 1.8 Ω following the growth of PANI (Figure 5c). This notable reduction in the charge transfer resistance is due to the penetration of concentrated H_2SO_4 and the growth of flake-like conducting PANI nanostructures. Consequently, the composite electrode possesses rapid electron transport and enhanced charge transfer kinetics, which is consistent with the findings from CV and GCD results. Moreover, the series resistance value of the SWCNTs shows only a slight increase from 1.67 to 2.22 Ω, suggesting that the composite electrode retains sufficient conductivity in the PANI component. This high conductivity allows rapid electrochemical reactions at surfaces and reactive sites between the electrodes and electrolytes. Thus, the CV curves exhibit a rapid response with reversible redox peak couples at different scan rates (Figure 5d). As the scan rate increases, the oxidation and reduction peaks shift positively and negatively, respectively, due to electrode resistance. In accordance with the CV curves, the GCD curves at different current densities display quasi-triangular shapes (Figure 5e), illustrating excellent reversible charging-discharging capacitive characteristics. In addition, a continuous conductive network in SWCNTs/PANI allows it to exhibit exceptional rate capability, achieving a high specific capacitance of 199 F g^{-1} at 10 A g^{-1} (Figure S14, Supporting Information). Moreover, the cycling stability of electrode materials is crucial for their practical application in the fabrication of high-performance SCs with long lifespans. The SWCNTs/PANI composite electrode exhibits remarkable long-term stability after 8000 cycles, exhibiting a retention percentage of 91.7%. This stability is ascribed to the successful formation of a continuous conductive network in the SWCNTs/PANI composite electrode. The high capacity of the SWCNTs/PANI electrode can be attributed to the following aspects: (1) the porous, flake-like PANI nanostructure facilitates the diffusion of electrolytic ions; (2) the direct growth of PANI on SWCNTs enables fast Faradaic reactions and enhances electronic conductivity; (3) the continuous conductive SWCNTs/PANI networks provide outstanding electron transfer capabilities; and

(4) the synergetic effect arising from the high electrical conductivity of SWCNTs and the elevated electrochemical activity of the PANI nanostructure contributes to the enhanced capacity.

In addition to their remarkable flexibility, freestanding SWCNTs/PANI films can be fabricated into high-performance solid-state devices. As illustrated in **Figure 6**a, the CV curves of the solid-state SC device constructed from SWCNTs/PANI display quasi-rectangular shapes, accompanied by weak redox peaks attributed to the pseudocapacitance of PANI. Furthermore, GCD curves were collected to evaluate the electrochemical performance of the SC device. As depicted in Figure 6b, the curves show nearly symmetric triangular shapes across various current densities, suggesting good electrochemical performance. Notably, a specific capacitance of 158.4 F g^{-1} is achieved at a current density of 0.5 A g^{-1}, which is comparable or even superior to that of other reported flexible SCs. Moreover, the continuous conductive network formed between the PANI and SWCNTs contributes to the SC's excellent cycling stability, its specific capacitance exhibited almost no loss even after 5000 cycles (Figure 6c). This high-performance device demonstrates remarkable mechanical stability and flexibility due to its self-supporting, integrated electrodes and compact design, achieving a thickness of ≈90 μm, as illustrated in Figure 6d. It can be bent in any direction while maintaining over 96.5% of its initial capacitance (Figure 6e and S15, Supporting Information), highlighting its significant potential for powering a wide range of portable electronic devices. In addition, the SC device exhibits a capacitance retention of 70.7% when the current density increases from 0.5 to 7 A g^{-1} due to the formation of a continuous conductive network between the PANI and SWCNTs.

To further characterize the capacitive performance, the energy and power densities of the solid-state SC were calculated. The Ragone plots presented in Figure 6f illustrate that a maximum energy density of 14 Wh kg^{-1} is achieved at a power density of 400 W kg^{-1}. This performance is comparable to, and in some cases exceeds that of various PANI-based SCs using different electrodes, such as the ACNTA-PANI/PDMS (8.3 Wh kg^{-1}, 1071 W kg^{-1}),[22] porous CNT sponge/PANI (14.87 Wh kg^{-1},
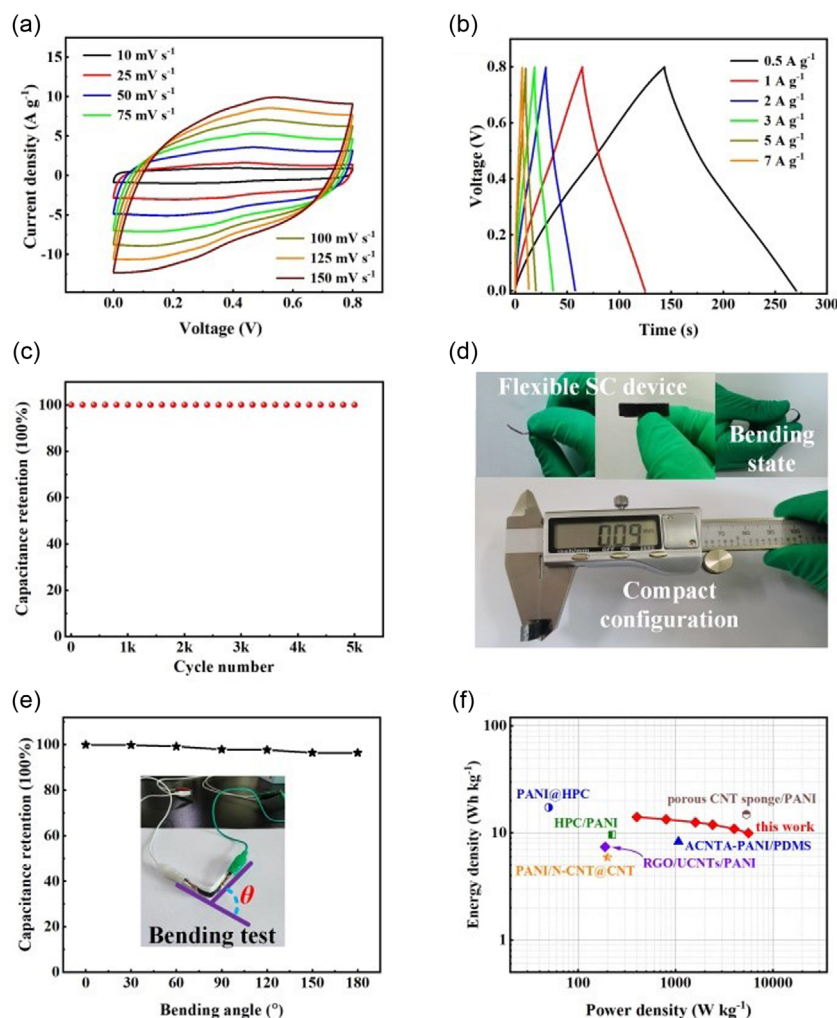
Figure 6. Electrochemical behaviors of the solid-state SC devices based on SWCNTs/PANI composite: a) CV curves of different scan rates; b) GCD curves at different current densities; c) cycle stability during the long-term charging/discharging test; d) photographs of a flexible SC based on SWCNTs/PANI film electrode and its compact configuration, with a thickness of 90 μm; e) capacitance retention at different bending angles; and f) Ragone plots of the SWCNTs/PANI-based solid-state SC and comparison to other SC devices.

5340 W kg^{-1}),[23] RGO/UCNTs/PANI (7.4 Wh kg^{-1}, 189 W kg^{-1}),[8] PANI/N-CNT@CNT (5.9 Wh kg^{-1}, 200 W kg^{-1}),[5d] PANI@HPC (17.3 Wh kg^{-1}, 49.8 W kg^{-1}),[24] and hierarchically porous carbon/PANI composite electrode (9.6 Wh kg^{-1}, 223 W kg^{-1}).[25] In addition, at a power density of 5603 W kg^{-1}, the energy density of the flexible SC device attains 10 Wh kg^{-1} at a current density of 7 A g^{-1}. These findings suggest that the SWCNT/PANI-based SC can simultaneously deliver both high energy and power densities, demonstrating its significant potential as an energy storage device.

3. Conclusion

A novel method was developed for fabricating flexible, large-area, and freestanding SWCNTs/PANI composite films employing a "direct-immersion strategy" for SC electrodes. Initially, PANI nanostructures were deposited on the surfaces of the SWCNTs film by soaking it in a PANI-H$_2$SO$_4$ solution. Through optimization of the experimental conditions, the composite film electrode achieved a

specific capacitance of 329 F g^{-1} with excellent cycling performance. In addition, an SC based on SWCNTs/PANI showcased a high energy density of 14 Wh kg^{-1} and a power density of 400 W kg^{-1}, outperforming many other relevant SCs. Moreover, the SC demonstrated excellent flexibility with no significant change in specific capacitance at different bending angles from 0 to 180°, even after hundreds of bending cycles at 180°. The characteristic indicates its considerable potential for practical applications. This work provides a novel strategy for fabricating reliable and efficient SWCNTs/PANI composite films, highlighting their promising applications in electrochemical devices.

4. Experimental Section

Materials

Aqueous dispersion of carboxylic ultrapure SWCNT with an outer diameter of 1–2 nm and a length of 5–30 μm (purity >95.0 wt%) was procured from XFNANO Materials Technology Co., Ltd. (Nanjing,

Batteries & Supercaps

Research Article
doi.org/10.1002/batt.202500063

Chemistry Europe
European Chemical
Societies Publishing

China). Aniline, ammonium persulfate (APS), ammonia solution (28−30%), PVA, hydrochloric acid (HCl, 35−38%), phosphoric acid (H_3PO_4, 85%), and sulfuric acid (H_2SO_4, 98%) were supplied by Beijing InnoChem Science & Technology Co., Ltd. Only aniline was purified by vacuum distillation, while all other reagents were used as received. Deionized (DI) water (resistance of ≈18.2 MΩ cm) was utilized during the sample preparation and testing processes.

Synthesis

To prepare the SWCNTs/PANI composite films, the process begins with the synthesis of conducting PANI powder. Initially, 1 mL of aniline was added to 90 mL of 1 M HCl to make a suspension. Next, 2.5 g of APS was dissolved in 100 mL of a 1 M HCl aqueous solution and directly mixed with the aforementioned suspension, followed by incubation at 0−5 °C for 8 h. The product was then purified sequentially using water and methanol. The collected PANI was stirred in a 0.1 M ammonia solution for 24 h at room temperature. Subsequently, DI water and methanol were used to filter and wash the PANI-suspended solution several times before vacuum drying at 60 °C for 24 h. The collected PANI was dried and ground into powder. To prepare the PANI-H_2SO_4 solution, 0.2 g of PANI powder was dissolved in 30 mL of concentrated H_2SO_4 after 2 h of sonication.

For fabrication of the SWCNTs/PANI composite film, a SWCNTs suspension (1.5 wt% SWCNTs in aqueous solution) was first diluted to 1 mg mL^{-1}. A volume of 100 μL of the diluted solution was drop-coated onto a precleaned glass slide (1.0 × 1.0 cm) and allowed to dry naturally under ambient conditions. The CNTs film was subsequently immersed in the as-prepared PANI-H_2SO_4 solution at different temperatures (−18, 5, 25, 30, and 40 °C) for different durations. After each treatment period, the sample was taken out from the PANI-H_2SO_4 solution, followed by a water-spraying process at room temperature. ≈80 μL of DI water was sprayed onto the sample surface each time. To control the amount of PANI deposited, this water-spraying process was conducted three times at 60 mins intervals under the same condition. We next removed the residue PANI-H_2SO_4 solution and thoroughly washed the composite film with DI water. Finally, the SWCNTs/PANI composite film was dried at room temperature and it was peeled off from the glass substrate.

Characterization

To examine the film morphology, field emission scanning electron microscopy (FE-SEM, Hitachi 4800, Hitachi Limited, Tokyo, Japan) and TEM (FEI Tecnai G^2 F20S-TWIN) were used. Raman spectra were recorded on a LabRAM HR Evolution instrument equipped with a 532 nm laser beam, covering a wavenumber range of 100−3000 cm^{-1}. A Lambda 950 UV/VIS/NIR Spectrometer was used to collect UV–Vis–NIR spectra within the wavelengths of 175−3300 nm. Molecular structures were also characterized by FTIR (Nicolet iS5, Thermo Fisher Scientific, Waltham, MA, USA) with a spectral scanning range of 400–4000 cm^{-1}. The binding energies of the elements in samples were determined using an XPS (Thermo KAlpha, Thermo Fisher Scientific, Shanghai, China). Chemical measurements were conducted on a CHI 660 E electrochemical workstation (Shanghai CH Instruments Co., China).

The electrochemical performance of the film electrodes was investigated using a three-electrode system in 1 M H_2SO_4. The working electrode comprised SWCNTs/PANI and SWCNTs films, with a saturated calomel electrode serving as the reference electrode and a Pt mesh as the counter electrode. For the traditional PANI, the working electrode was formulated from PANI powder, acetylene black, and the binder polytetrafluoroethylene in a weight ratio of 8:1:1. CV and GCD measurements were performed at various scan rates across a potential range from −0.2 to 0.8 V. Additionally, EIS was performed in the frequency range of $10^5−10^{-2}$ Hz with an amplitude of 5 mV. The specific capacitance (C_s) of the film electrodes was calculated using the equation: $C_s = It/m\Delta V$, where I represents the constant discharge current (A), t represents the discharge time (s), m denotes the mass of the integrated film electrode (g), and ΔV stands for the potential window (V).

For the fabrication of the solid-state SC device, a PVA/H_3PO_4 electrolyte was prepared using the following method: a mixture of 5 g of PVA and 3 mL of H_3PO_4 was mixed with 45 mL DI water and heated to 95 °C with continuous stirring until a transparent solution was obtained. Two film electrodes were coated with a suitable thickness of the PVA/H_3PO_4 electrolyte and dried under vacuum at room temperature. Subsequently, the electrodes were pressed together to form an SC, with the PVA/H_3PO_4 serving as both the polymer electrolyte and the separator.

The specific capacitance of the solid-state SC device (C_{ss}) was calculated from the GCD curves using the equation: $C_{ss} = 2It/m\Delta V$, where I, t, m, and ΔV represent the constant discharge current, discharge time, mass of single-film electrode, and discharge potential window, respectively. The energy density (E_m, Wh kg^{-1}) and power density (P_m, W kg^{-1}) of the SC device were determined using $E_m = 0.5C_{ss}\Delta V^2/3600$ and $P_m = 3600 E_m/t$, respectively. Here, C_{ss} denotes the specific capacitance of the device, ΔV represents the potential window, and t signifies the discharge time.

Conflict of Interests

The authors declare no conflict of interest.

Data Availability Statement

The data that support the findings of this study are available from the corresponding author upon reasonable request.

Batteries & Supercaps

Research Article
doi.org/10.1002/batt.202500063

Chemistry Europe
European Chemical
Societies Publishing

[1] a) F. Xing, Z. Bi, F. Su, F. Liu, Z. S. Wu, *Adv. Energy Mater.* **2022**, *12*, 2200594; b) W. Zhang, Y. Huang, Y. Liu, L. Wang, S. Chou, H. Liu, *Adv. Energy Mater.* **2019**, 1900464; c) Y. Huang, M. Zhu, W. Meng, W. Fu, Z. Wang, Y. Huang, Z. Pei, C. Zhi, *RSC Adv.* **2015**, *5*, 33981; d) R. Coneo-Rodríguez, A. Y. Tesio, F. P. Cometto, G. M. Morales, G. Á. Planes, A. Caballero, *Batteries Supercaps* **2024**, *8*, e202400502.

[2] a) Y. Jiang, J. Ou, Z. Luo, Y. Chen, Z. Wu, H. Wu, X. Fu, S. Luo, Y. Huang, *Small* **2022**, *18*, 2201377; b) J. Zihe, H. Xuebo, X. Lijuan, X. Z. YanpingZongwen, Z. Zongwen, *J. Xinyang Norm. Univ. (Nat. Sci. Ed.)* **2023**, *36*, 540.

[3] a) Y. Xu, Z. Yao, A. Liu, G. Shi, *ACS Nano* **2010**, *4*, 1963; b) X. Wang, D. Wu, X. Song, W. Du, X. Zhao, D. Zhang, *Molecules* **2019**, *24*, 2263.

[4] a) H. Cheng, J. Li, T. Meng, D. Shu, *Small* **2023**, *20*, 2308804; b) L. Fuwei, G. Luyao, D. Yuqing, D. Jiajia, L. Huiying, W. Mengke, L. Fuqun, L. Ruotong, Z. Chao, L. Shenghong, *J. Xinyang Norm. Univ. (Nat. Sci. Ed.)* **2024**, *37*, 24; c) I. Hussain, D. Mohapatra, G. Dhakal, C. Lamiel, S. G. Mohamed, M. S. Sayed, J.-J. Shim, *J. Energy Storage* **2020**, *32*, 101767.

[5] a) R. B. Choudhary, S. Ansari, B. Purty, *J. Energy Storage* **2020**, *29*, 101302; b) D. J. Ahirrao, A. K. Pal, V. Singh, N. Jha, *J. Mater. Sci.Technol.* **2021**, *88*, 168; c) L. Fuwei, G. Luyao, C. Xue, W. Letian, C. Qinru, C. Zhiwei, Z. Chao, X. Wenhe, *J. Xinyang Norm. Univ. (Nat. Sci. Ed.)* **2023**, *36*, 380; d) J. Tian, N. Cui, P. Chen, K. Guo, X. Chen, *J. Mater. Chem. A* **2021**, *9*, 20635.

[6] a) F. Li, J. Shi, X. Qin, *Chin. Sci. Bull.* **2010**, *55*, 1100; b) H. Xu, L. Cui, X. Pan, Y. An, X. Jin, *Int. J. Biol. Macromol.* **2022**, *219*, 1135.

[7] H. Wang, D. Liu, P. Du, P. Liu, *Electrochim. Acta* **2018**, *289*, 104.

[8] Y. Huang, J. Zhou, N. Gao, Z. Yin, H. Zhou, X. Yang, Y. Kuang, *Electrochim. Acta* **2018**, *269*, 649.

[9] Z. Niu, P. Luan, Q. Shao, H. Dong, J. Li, J. Chen, D. Zhao, L. Cai, W. Zhou, X. Chen, S. Xie, *Energy Environ. Sci.* **2012**, *5*, 8726.

[10] a) L. Dong, G. Liang, C. Xu, D. Ren, J. Wang, Z.-Z. Pan, B. Li, F. Kang, Q.-H. Yang, *J. Mater. Chem. A* **2017**, *5*, 19934; b) X. Li, Y. Li, S. Xie, Y. Zhou, J. Rong, L. Dong, *Chem. Eng. J.* **2022**, *427*, 131799.

[11] Q. Cheng, C. Yang, L. Han, K. Tao, *Batteries Supercaps* **2020**, *3*, 370.

[12] a) H. Liu, Y. He, K. Cao, *Adv. Mater. Interfaces* **2021**, *8*, 2100982; b) S. Haibin, L. Shuangshuang, Z. Huiru, F. Can, W. Qingqing, L. Gaoli, *J. Xinyang Norm. Univ. (Nat. Sci. Ed.)* **2022**, *35*, 108.

[13] L. Bokobza, J. Zhang, *Express Polym. Lett.* **2012**, *6*, 601.

[14] a) D. Xing, M. Rana, B. Hao, Q. Zheng, P.-C. Ma, *Electrochim. Acta* **2022**, *427*, 140847; b) A. Kumar Sharma, P. Kumar Jain, R. Vyas, V. Mathur, V. Kumar Jain, *Mater. Today: Proc.* **2021**, *38*, 1259; c) F. Liu, L. Xie, L. Wang, W. Chen, W. Wei, X. Chen, S. Luo, L. Dong, Q. Dai, Y. Huang, L. Wang, *Nano-Micro Lett.* **2020**, *12*, 17.

[15] X. Li, C. Zhang, S. Xin, Z. Yang, Y. Li, D. Zhang, P. Yao, *ACS Appl. Mater. Interfaces* **2016**, *8*, 21373.

[16] Q. Yao, Q. Wang, L. Wang, L. Chen, *Energy Environ. Sci.* **2014**, *7*, 3801.

[17] L. Wang, Q. Yao, J. Xiao, K. Zeng, S. Qu, W. Shi, Q. Wang, L. Chen, *Chem.–Asian J.* **2016**, *11*, 1804.

[18] a) M. Abdolkarimi-Mahabadi, A. Bayat, A. Mohammadi, *Theor. Exp. Chem.* **2021**, *57*, 191; b) G. A. Rance, D. H. Marsh, R. J. Nicholas, A. N. Khlobystov, *Chem. Phys. Lett.* **2010**, *493*, 19.

[19] R. Chan Yu King, F. Roussel, J.-F. Brun, C. Gors, *Synth. Met.* **2012**, *162*, 1348.

[20] a) M. Ghasem Hosseini, E. Shahryari, *J. Colloid Interf. Sci.* **2017**, *496*, 371; b) Y. Li, X. Li, R. Zhao, C. Wang, F. Qiu, B. Sun, H. Ji, J. Qiu, C. Wang, *Mater. Sci. Eng. C* **2017**, *72*, 106.

[21] F. Liu, S. Luo, D. Liu, W. Chen, Y. Huang, L. Dong, L. Wang, *ACS Appl. Mater. Interfaces* **2017**, *9*, 33791.

[22] R. D. C. Balboni, G. K. Maron, M. G. Masteghin, M. O. Tas, L. S. Rodrigues, V. Gehrke, J. H. Alano, R. Andreazza, N. L. V. Carreño, S. R. P. Silva, *Nanoscale* **2022**, *14*, 2266.

[23] W. Zhao, Y. Li, S. Wu, D. Wang, X. Zhao, F. Xu, M. Zou, H. Zhang, X. He, A. Cao, *ACS Appl. Mater. Interfaces* **2016**, *8*, 34027.

[24] Y. Zhao, Z. Zhang, Y. Ren, W. Ran, X. Chen, J. Wu, F. Gao, *J. Power Sources* **2015**, *286*, 1.

[25] F. Miao, C. Shao, X. Li, K. Wang, N. Lu, Y. Liu, *J. Power Sources* **2016**, *329*, 516.

[26] S. Yu, D. Liu, S. Zhao, B. Bao, C. Jin, W. Huang, H. Chen, Z. Shen, *RSC Adv.* **2015**, *5*, 30943.

[27] X. Zhou, L. Li, S. Dong, X. Chen, P. Han, H. Xu, J. Yao, C. Shang, Z. Liu, G. Cui, *J. Solid State Electr.* **2011**, *16*, 877.

[28] Y. Hu, X. Tong, H. Zhuo, L. Zhong, X. Peng, *ACS Sustainable Chem. Eng.* **2017**, *5*, 8663.

[29] S. K. Simotwo, C. DelRe, V. Kalra, *ACS Appl. Mater. Interfaces* **2016**, *8*, 21261.

[30] A. P. M. Udayan, O. Sadak, S. Gunasekaran, *ACS Appl. Energy Mater.* **2020**, *3*, 12368.

[31] M. Hassan, K. R. Reddy, E. Haque, S. N. Faisal, S. Ghasemi, A. I. Minett, V. G. Gomes, *Compos. Sci. Technol.* **2014**, *98*, 1.

[32] K. Zhang, L. L. Zhang, X. S. Zhao, J. Wu, *Chem. Mater.* **2010**, *22*, 1392.